View metadata, citation and similar papers at core.ac.uk

brought to you by CORE

provided by Digital Repository @ Iowa State University

IOWA STATE UNIVERSITY
Digital Repository

Mechanical Engineering Publications | Mechanical Engineering

6-2020

Leidenfrost behavior in drop-wall impacts at combustor-relevant ambient pressures

Abhijeet Chausalkar
Iowa State University

Chol-Bum M. Kweon
United States Army Research Laboratory

Song-Charng Kong
Iowa State University, kong@iastate.edu

James B. Michael
Iowa State University, jmichael@iastate.edu

Follow this and additional works at: https://lib.dr.iastate.edu/me_pubs

 Part of the Heat Transfer, Combustion Commons

The complete bibliographic information for this item can be found at https://lib.dr.iastate.edu/me_pubs/442. For information on how to cite this item, please visit http://lib.dr.iastate.edu/howtocite.html.

This Article is brought to you for free and open access by the Mechanical Engineering at Iowa State University Digital Repository. It has been accepted for inclusion in Mechanical Engineering Publications by an authorized administrator of Iowa State University Digital Repository. For more information, please contact digirep@iastate.edu.

Leidenfrost behavior in drop-wall impacts at combustor-relevant ambient pressures

Abstract

Liquid-fueled combustion systems demand optimal performance over a range of operating conditions—requiring predictable fuel injection events, spray breakup, and vaporization across a range of temperatures and pressures. In direct injection combustors, these sprays impinge directly on combustion chamber surfaces. Although the outcome of fuel droplets impacting a wall is primarily driven by the wall temperature and the Leidenfrost effect, the shifting liquid-vapor saturation point with pressure may influence the droplet-wall heat transfer rate and transition from nucleate to film boiling. In this paper, the role of ambient pressure on the droplet impact regimes, spreading rate, and droplet rebound velocity during impact are explored for representative low boiling point and high boiling point pure hydrocarbon liquids (n-heptane and n-decane). High-speed image sequences of the drop-wall impact were acquired for ambient pressures of 1–20 bar and wall temperatures ranging from 35–300 ◦C with a drop Weber number of ~ 50. Droplet impact sequences were recorded using a high-speed CMOS camera and were processed to measure the droplet spread, droplet rebound velocity and track the droplet centroid motion. The dynamics of the drop spreading and rebound show similar behavior across a range of ambient pressures with the largest differences observed for wetted versus non-wetted cases (above the Leidenfrost temperature). For both fluids, the onset of drop rebound remains bounded by the saturation temperature (shifting with ambient pressure) and the thermodynamic limit of liquid superheat. This leads to a decrease in the superheat temperature above the saturation point as the critical pressure is approached.

Keywords

Drop-wall impact, Film boiling, Leidenfrost effect

Disciplines

Heat Transfer, Combustion | Mechanical Engineering

Comments

This article is published as Chausalkar, Abhijeet, Chol-Bum M. Kweon, Song-Charng Kong, and James B. Michael. "Leidenfrost behavior in drop-wall impacts at combustor-relevant ambient pressures." *International Journal of Heat and Mass Transfer* 153 (2020): 119571. DOI: 10.1016/j.ijheatmasstransfer.2020.119571.

This article is available at Iowa State University Digital Repository: https://lib.dr.iastate.edu/me_pubs/442

International Journal of Heat and Mass Transfer 153 (2020) 119571

Contents lists available at ScienceDirect

International Journal of Heat and Mass Transfer

journal homepage: www.elsevier.com/locate/hmt

Leidenfrost behavior in drop-wall impacts at combustor-relevant ambient pressures

Abhijeet Chausalkar[a], Chol-Bum M. Kweon[b], Song-Charng Kong[a], James B. Michael[a,*]

[a] Department of Mechanical Engineering, Iowa State University, Ames, IA 50011, United States
[b] Vehicle Technology Directorate, U.S. Army Combat Capabilities Development Command (CCDC) Army Research Laboratory, APG, MD, United States

ARTICLE INFO

Article history:
Received 20 August 2019
Revised 10 January 2020
Accepted 23 February 2020
Available online 8 March 2020

Keywords:
Drop-wall impact
Film boiling
Leidenfrost effect

ABSTRACT

Liquid-fueled combustion systems demand optimal performance over a range of operating conditions—requiring predictable fuel injection events, spray breakup, and vaporization across a range of temperatures and pressures. In direct injection combustors, these sprays impinge directly on combustion chamber surfaces. Although the outcome of fuel droplets impacting a wall is primarily driven by the wall temperature and the Leidenfrost effect, the shifting liquid-vapor saturation point with pressure may influence the droplet-wall heat transfer rate and transition from nucleate to film boiling. In this paper, the role of ambient pressure on the droplet impact regimes, spreading rate, and droplet rebound velocity during impact are explored for representative low boiling point and high boiling point pure hydrocarbon liquids (n-heptane and n-decane). High-speed image sequences of the drop-wall impact were acquired for ambient pressures of 1–20 bar and wall temperatures ranging from 35–300 °C with a drop Weber number of ~ 50. Droplet impact sequences were recorded using a high-speed CMOS camera and were processed to measure the droplet spread, droplet rebound velocity and track the droplet centroid motion. The dynamics of the drop spreading and rebound show similar behavior across a range of ambient pressures with the largest differences observed for wetted versus non-wetted cases (above the Leidenfrost temperature). For both fluids, the onset of drop rebound remains bounded by the saturation temperature (shifting with ambient pressure) and the thermodynamic limit of liquid superheat. This leads to a decrease in the superheat temperature above the saturation point as the critical pressure is approached.

© 2020 Elsevier Ltd. All rights reserved.

1. Introduction

Gas-turbine combustors and internal combustion engines operate over a range of high ambient pressure and temperature conditions. In compression-ignition systems (Diesel), typical in-cylinder pressures vary from 35–150 bar during the compression cycle and piston wall temperatures range from 200–300 °C [1]. Similarly, in gas turbines, chamber pressure and temperature vary from 10–50 bar [2]. In these combustors, fuels such as gasoline, diesel, or aviation kerosene (Jet-A) are typically multicomponent and are injected at high pressure to achieve rapid mixing and combustion–necessary for high fuel economy and cycle efficiency. These high-pressure injections result in rapid atomization of liquid fuel into microscale droplets and ensure high surface to volume ratio for optimal vaporization, mixing, and heat release [3,4]. Following injection, droplets travel at a range of velocities to impinge on the hot valve stem (indirect fuel injection) or piston crown walls (direct fuel injection). The outcome of the spray impingement on walls across a range of temperatures and ambient pressures can significantly influence the ultimate air-fuel mixture quality, as individual droplets may wet the wall, rebound, or breakup upon impact. The ultimate rebound or deposition of these drops on the combustor wall can also play a significant role in the overall pollutant emissions from the combustor. For cold-start operation, the formation of a thin fuel film on the inlet valve surface or piston crown top contributes to unburned hydrocarbon emissions in the engine exhaust [3,5]. Understanding the drop-wall impact dynamics and ultimate outcomes is necessary to establish predictive modeling capabilities for the full range of ambient pressure and wall temperature conditions.

Drop-wall impact outcomes on high temperature walls have been examined for a number of fluids and impact conditions, allowing classification into a small number of distinct regimes [6–11]. These regimes can be classified into those where vapor formation at the wall limits liquid-wall contact and may result in rebound (i.e., Leidenfrost effects), cases where the drop wets the

* Corresponding author.
E-mail address: jmichael@iastate.edu (J.B. Michael).

https://doi.org/10.1016/j.ijheatmasstransfer.2020.119571
0017-9310/© 2020 Elsevier Ltd. All rights reserved.

wall, and cases where the drop momentum is sufficient to drive secondary breakup and atomization. Splashing and drop breakup occurs for sufficiently high impact velocity at both low and high wall temperature [6,12,13]. To summarize the classification of impact regimes previously identified at atmospheric pressure, four distinct categories have been identified for a single fluid and fixed saturation temperature [14]. By comparing fluid-specific temperature points with the wall temperature, these are classified as film evaporation ($T_w < T_{sat}$); nucleate boiling ($T_{sat} < T_w < T_{Nukiyama}$); transition boiling ($T_{Nukiyama} < T_w < T_L$); and film boiling ($T_w > T_L$). Here, T_w is the wall temperature and T_{sat} is the liquid saturation temperature. T_L is the Leidenfrost temperature corresponding to the temperature of minimum heat flux for a near-stationary drop, and $T_{Nukiyama}$ corresponds to the maximum heat flux [15]. In the film evaporation regime, where the wall temperature is below the saturation temperature, the droplet spreads on the surface and forms a thin liquid film [10,16]. As the wall temperature increases to the saturation temperature, small-scale droplets are ejected from the surface of the liquid film as the result of bubble formation at wall nucleation sites, defining the nucleate boiling regime. The film boiling regime is characterized by the presence of a vapor layer between the hot wall and the liquid film and results in drop rebound for low impact momentum. This point is often identified with the Leidenfrost temperature or the dynamic Leidenfrost temperature, where the heat transfer rate reaches a minimum as all heat conducts through the vapor layer.

At elevated pressure, Temple et al.[17], Hiroyasu et al.[18], and Emmerson and Snoek[19] examined the Leidenfrost point behavior of pure fluids. These studies reported increasing Leidenfrost temperature with increasing pressure based on the total duration of liquid drop vaporization on a hot wall. Temple et al.[17] reported two distinct outcomes: a contact mode and a spheroidal evaporation mode [17]. In the contact mode ($T_w < T_{sat}$), the drop remains in contact with the wall and maintains a convex shape through the vaporization process. In the spheroidal evaporation mode ($T_w > T_{sat}$), the drop floats over the vapor cushion as the wall temperature is significantly higher than the Leidenfrost point. Interestingly, several of these studies examined the excess wall temperature above the saturation temperature ($T_w - T_{sat}$) as a function of pressure, and found minimal variation. These studies focused on the duration of wall contact based on the global heat transfer rate, but did not examine the dynamics of the drop-wall interaction. Buchmüller et al.[20] also reported the impact of water drops for pressures of 1–25 bar and wall temperatures from 100–460 °C for near-stationary drops (*We* of 5). These results showed four impact outcomes (wetted, wetted boiling, transition boiling, and rebound) and their results suggest a decrease in the range of transition boiling with increasing pressure. These experimental studies have yet to establish consensus on the Leidenfrost temperature trend with increasing pressure, particularly across multiple pure fluids and large ambient pressure ranges.

For prediction of the Leidenfrost temperature corresponding to maximum heat transfer rate or the temperature of rebound (the Leidenfrost temperature in this study), consideration of the maximum temperature of liquid superheat is of interest. There are two relevant definitions which have been examined in some detail: the thermodynamic limit of superheat and the kinetic limit of superheat [21–23]. These concepts are relevant to phenomena of rapid depressurization (bubble nucleation in cavitation) and rapid heating (liquid superheating in boiling) and define the existence limit for a metastable, superheated liquid state. We will limit our discussion to the thermodynamic limit of superheat, defined by $\frac{\partial p}{\partial v}|_T$, which is reviewed by Katz and Blander [22]. As reviewed by Liang and Mudawar in the context of the Leidenfrost temperature, the limit of liquid superheat has not been found a sufficient predictor of the Leidenfrost temperature, but nevertheless gives an indication of the upper limits for liquid metastable states [21]. Eberhart examined n-alkanes using two-constant equations of state, and found a limit of superheat of approximately 80 percent of the critical temperature. The idea of the superheat of the liquid also governs heat transfer, and correlations based on the Jakob number are often used [24,25]. The Jakob number (*Ja*) represents the ratio of the sensible heat to the latent heat of vaporization, while the Stefan (*Ste*) number represents the fraction of energy available for complete phase transition. They are given by

$$Ja = \frac{\rho_f}{\rho_g}\frac{c_{p,f}(T - T_{sat})}{h_{fg}} \tag{1}$$

and

$$Ste = \frac{c_{p,f}(T - T_{sat})}{h_{fg}} = Ja\frac{\rho_g}{\rho_\ell}, \tag{2}$$

where T represents the liquid superheat temperature, T_{sat} represents the saturation temperature, h_{fg} the enthalpy of vaporization, and ρ_f and ρ_g the saturated liquid and saturated vapor density, respectively.

The dynamics of drop impact are also important in the context of heat transfer modeling and combustion spray-wall modeling. At low impact velocities and high wall temperature, drops recoil and rebound, but at higher impact velocities secondary droplets are generated due to prompt/corona splashing and disintegration of the vapor-cushioned liquid film above the hot wall [10,13,16,26]. These outcomes are the result of complex interplay of thermal, fluid and momentum parameters. To consider the effects of varying ambient pressure, it is useful to examine the variation of physical properties. The non-dimensional parameters typically used to characterize drop-wall interactions consist of the Reynolds, Ohnesorge, and Weber numbers. The Reynolds number, defined as

$$Re = \frac{\rho_f U_0 d_0}{\mu_f}, \tag{3}$$

describes the ratio of inertial to viscous forces acting on the drop, where physical quantities are the liquid density (ρ_f), the initial drop diameter (d_0), the liquid viscosity (μ_f), and the wall normal velocity at impact (U_0). The Ohnesorge number describes the ratio of viscous forces to the combined inertial and surface tension forces and is defined as

$$Oh = \frac{\mu_f}{\sqrt{\rho_f \sigma d_0}}, \tag{4}$$

where σ is the liquid-vapor surface tension. The third non-dimensional parameter commonly used in classifying drop-wall interactions is the Weber number, which describes the relative effects of the liquid drop inertia and surface tension. It can be expressed in terms of *Oh* and *Re* as

$$We = Oh \cdot Re^2 = \frac{\rho_f U_0^2 d_0}{\sigma}. \tag{5}$$

Over the ambient pressure range under study here (1–20 bar) and ambient temperature (25 °C), the variation in Weber number due to surface tension, liquid viscosity, and liquid density is approximately 8%, with the surface tension reducing by ~ 14 %. As a result, the variation in outcomes was expected to be dominated by the enthalpy of vaporization and shifting saturation temperature, as opposed to variations in the liquid physical properties.

This paper presents experimental characterization of drop-wall impacts of pure fluids (n-alkanes) with hot walls (35–300 °C) for ambient pressures from 1–20 bar. These conditions span ambient pressure conditions seen in internal combustion engines and gas turbine combustion systems. Impact sequences of n-heptane and

n-decane are mapped for a range of wall temperatures and ambient pressures. The morphological changes of the drop, the dynamic spreading of the liquid film, and the rebound regime boundaries are compared for n-heptane and n-decane, which serve as analogs for low- and high-boiling point liquids typically found in transportation fuels. The onset of drop rebound is compared to the limit of liquid superheat. The dynamics of drop spreading and rebound at elevated pressure are also examined to provide experimental data for drop-wall modeling over a range of ambient pressure conditions.

2. Experimental setup

Experiments were carried out in a constant-volume pressure vessel rated to 100 bar, as shown in Fig. 1. The vessel consists of a 175-mm inner diameter cylinder with a height of ~ 450 mm, and has four-sided optical access. The vessel walls are 316 stainless steel and the total volume is 0.01 m^3. Optical access for backlit imaging was provided through opposed 76-mm diameter, 19-mm thick quartz windows. For high pressure operation, a safety relief valve was set at 30 bar and nitrogen gas was supplied from a N_2 compressed gas cylinder. A micro-precision orifice with a 0.226-mm diameter was used to maintain a sweep gas flow rate of 10 L/min to evacuate any residual fuel vapor within a few minutes. A syringe pump (New Era NE-8000) was used to generate drops with diameters of 1.8–2.0 mm from a 28-gauge needle (nominal inner diameter 0.159 mm). The volume of the drop generated was 3.68 mm^3, with minimal variation in diameter and volume with ambient pressure changes. The needle was set 75 mm above the wall surface. After generation, the droplet fell through the ambient gas onto a smooth aluminum substrate of 25.4 × 25.4 mm^2 with a thickness of 12.5 mm. Based on five measurement sets, the substrate roughness parameters R_a, and R_z are 1.53 µm, 12.768 µm respectively. The roughness of the test surfaces was measured using an 3D optical surface profiler (Zygo, NewView 7100). The aluminum substrate is heated to a temperature of up to 400 °C by a square-profile 1-kW heater of the same area (25.4 × 25.4 mm^2) with a thickness of 2.48 mm (CER-1-01-00002). The wall and heater assembly are shown in the inset of Fig. 1.

The aluminum substrate and flat heater were secured inside a ceramic insulator to limit heat transfer to the surrounding gas and achieve the maximum possible wall temperature. The heater was controlled with an embedded K-type thermocouple and a Watlow PID controller. The wall temperature was verified using three 1.58-mm K-type thermocouples embedded in the aluminum substrate with a vertical spacing of 6.3 mm to confirm one-dimensional, steady-state heat transfer. Three additional thermocouples were installed at different locations in the vessel to monitor the vessel ambient gas temperature, the temperature of the liquid injector cooling jacket, and the gas temperature near the injection location. The location of these thermocouples is shown in Fig. 1. In order to maintain constant liquid injection temperatures, a counterflow cooling jacket was designed to maintain the temperature of the liquid at room temperature. The cooling jacket consisted of the fuel tube surrounded by two additional concentric tubes. The liquid temperature was maintained by circulating air at a mass flow rate between 70-100 slpm to maintain the liquid injection temperature. The cooling jacket was designed using two stainless tubes of inner diameter 19.05 mm and 3.175 mm, respectively. The cooling jacket was installed in the pressure vessel top flange using a bulkhead compression fitting. The temperatures reported in the paper are steady-state values, measured over 60 s prior to drop injection. All thermocouple temperatures were recorded with a data acquisition system (LabJack T7-Pro).

High-speed backlit image sequences of each drop impact were recorded with a high-speed complementary metal-oxide semiconductor (CMOS) camera (Photron FASTCAM SA-X2). A 1500-grit ground glass diffuser and a halogen lamp (500 W) were used for back illumination of the droplets. Images were recorded using an f/2.8 105-mm focal length lens with a 72-mm lens extension (Nikon Nikkor). The measured field of view and depth of field were 24 × 22 mm^2 and 22 mm, respectively. Images were acquired as uncompressed TIFFs at a frame rate of 20 kHz and with a shutter exposure of 26 µs, yielding a frame size of 1020 × 672 $pixels^2$. Image processing was implemented in MATLAB for measurement of the spread of the liquid film and centroid location of the drop. Images were normalized using a background image, and the liquid location was identified using edge detection by a Canny algorithm [27]. Edges are dilated and eroded, and the resulting closed object is used to track to liquid extent and position. The time of first contact ($t = 0$ s), where droplet is about to impact the wall, is identified by tracking the droplet centroid acceleration or the second time-derivative of the major and minor axes. The velocity and drop diameter prior to impact were measured from the backlit images. The liquid spread extent is determined by the maximum extent of the identified object. A similar image processing procedure is used to identify the centroid and velocity of the rebounding drop.

For testing, the desired ambient pressure was first established in a cold vessel with a regulated N_2 gas supply. After the pressure of the vessel was steady, the wall temperature was raised to the test temperature. After achieving steady-state conditions, droplets were generated using the syringe pump at the liquid flow rate of 0.4–0.5 mL min^{-1}. The fuel flow rate was kept constant throughout the experiment. Test conditions with n-heptane and n-decane spanned wall temperatures from 21–300°C and pressures from 1–20 bar.

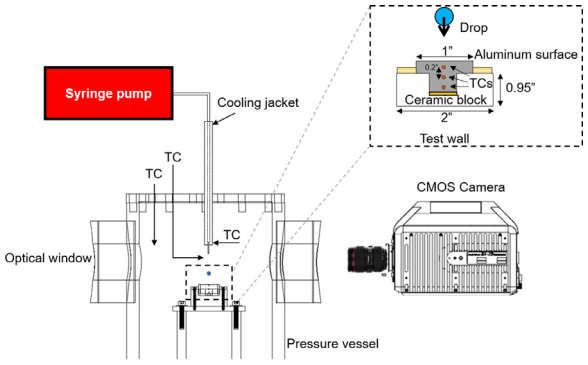

Fig. 1. Schematic of constant-volume pressure vessel showing the high-speed backlit imaging system and droplet injection apparatus. The inset shows a detailed view of the drop injection and substrate. Thermocouple locations are indicated by TC.

3. Results

In this section, experimental results of single-component liquids impacting walls are presented for two fluids over a range of wall temperatures (21–300 °C) and ambient pressures (1–20 bar). In all cases, the impact velocities are low, with a corresponding Weber number of ~ 50. First, the impact outcomes of experiments with n-heptane are compared for ambient pressure and elevated pressure. These outcomes are mapped onto a regime diagram, showing the onset of nucleate boiling and drop rebound for a range of ambient pressures. The transition in outcomes with increasing ambient pressure is compared to the thermodynamic limit of superheat, and variation of the dimensionless Jakob number. The extent of liquid film spreading and total drop rebound times are compared across these conditions in the subsequent section. The outcome of the drop-wall interactions will be described in Section 3.1, and the

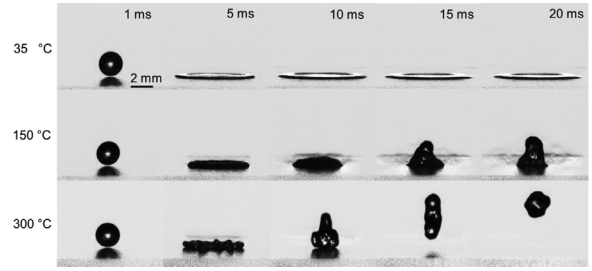

Fig. 2. Image sequences showing n-heptane drops impacting an aluminum substrate for wall temperatures of 35, 150, and 300 °C at 1 bar ambient pressure.

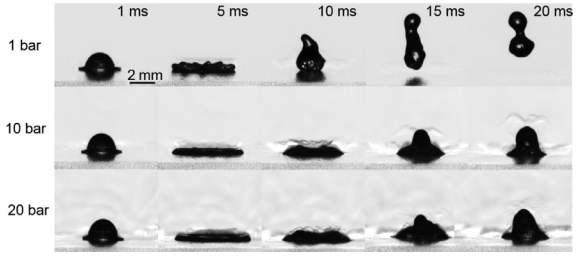

Fig. 3. Image sequences showing impact dynamics of n-heptane drops on an aluminum wall at a temperature of 200 °C in the ambient pressure range of 1–20 bar.

dynamics of the drop spreading and rebound will be described in Section 3.2.

3.1. Characterizing the impact of single-component liquids at elevated pressure

The impact of n-heptane drops on an aluminum wall are classified by the regimes mentioned previously, where rebound was observed for elevated wall temperatures ($T_w > > T_{sat}$). At low wall temperature, the liquid drop contacts the wall, spreads as a thin film, and undergoes slow evaporation. At higher temperatures (well above the saturation temperature), phase change at the interface results in rapid vapor production and the ultimate rebound of the drop. Fig. 2 shows a series of stills from high-speed image sequences of n-heptane drops impacting at 1 bar ambient pressure. In the top row, the sequence shows film spreading for a wall temperature of 35 °C. At $T_w = 150$ °C, the drop recoils but does not rebound, and at $T_w = 300$ °C, the drop spreads, recoils, and then rebounds away from the wall. This result corresponds closely with the dynamics and onset of drop rebound reported in the literature for n-heptane, and is classified as a film boiling regime [10,16,28]. The rebound temperature for a near-stationary n-heptane drop on a stainless steel surface has been previously reported as 200 °C, with the corresponding saturation temperature at 1 bar of 98.5 °C [16].

As the ambient pressure is increased, these outcomes shift to higher wall temperatures as expected from the variation in thermodynamic saturation point and liquid superheat limit. At a wall temperature of 100 °C for pressures of 1–20 bar (just above the saturation temperature at 1 bar), the drop impacts and deposits as a liquid film on the wall. At higher wall temperatures (above 100 °C), the effect of ambient pressure becomes prominent as the saturation temperature shifts. Fig. 3 shows comparison sequences for $T_w = 200$ °C, where the outcome shifts from film boiling (droplet rebound) at 1 bar to the film evaporation at 10 and 20 bar. Still frames from 1–20 ms after impact are shown in Fig. 3 where each row corresponds to a different ambient pressure case. In the upper row ($p = 1$ bar), the n-heptane drop spreads on the wall, then recoils and finally rebounds away from the wall. At 10 bar (the second row), bubble nucleation is evident in the liquid

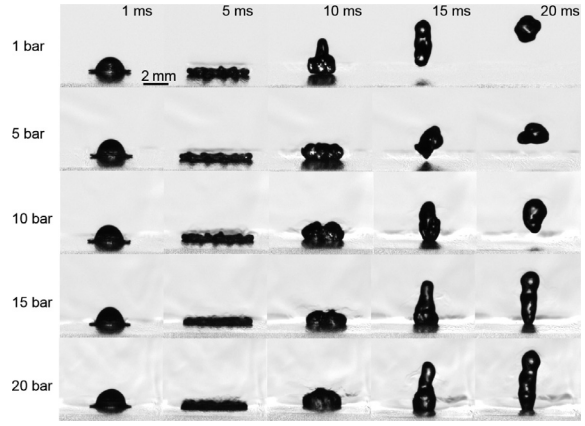

Fig. 4. Image sequences showing n-heptane drops impacting a 300 °C aluminum wall with varying ambient pressure (1–20 bar). Increase in ambient pressure delays the onset of drop rebound.

bulk for frames after 10 ms. Droplet ejections from the boiling liquid are observed late in time although not shown in these time snapshots, and the regime is characterized as nucleate boiling. The last row of Fig. 3, at 20 bar and a wall temperature of 200 °C, is classified as film evaporation. Here, the the liquid film spreads and recoils slowly, but remains deposited on the wall. This shift in the regime for a wall temperature of 200 °C with increasing ambient pressure corresponds to the saturation temperature variation from 98.5 °C (1 bar) to 245 °C (20 bar).

The variation with ambient pressure is also shown for n-heptane drops impacting at $T_w = 300$ °C in Fig. 4. Each horizontal row shows the drop evolution for indicated pressures of 1–20 bar. At all ambient pressures, the drop ultimately rebounds (film boiling regime), but the rebound is significantly delayed for increasing ambient pressure (for 15 and 20 bar, the drop rebounds after 20 ms). During liquid film spreading, the temperature of the liquid portion in contact with hot wall vaporizes to film a thin vapor layer cushion. After achieving the maximum extent, the liquid film begins to slip over the newly formed thin vapor layer resulting in a recoil motion. There are two factors contributing to the delayed rebound of drops at elevated pressure (but temperatures still above the Leidenfrost point): First, at constant wall temperature, the rate of vapor formation decreases with increasing pressure (and corresponding increase in the saturation temperature). Second, the local gas density has increased by an order of magnitude, leading to a shift in the force balance between the evolved vapor at the wall and the ambient gas. This variation in rebound characteristics will be discussed further by comparing the centroid location of the liquid mass after wall contact in Section 3.2.

The behavior of n-heptane drops impacting a heated wall are summarized by a regime map, as shown in Fig. 5. Here, the ambient pressure was varied from 1–20 bar and the wall temperature was varied from 35–300 °C while holding the impact velocity and Weber number constant ($We \sim 50$). In the regime map, impacts are classified into the three typical outcomes: film evaporation, nucleate boiling and transition, and film boiling as indicated by the symbols. Each point indicated on the regime map was confirmed by at least ten impact sequences at identical wall temperatures and ambient pressures. Also indicated are the saturation temperature (dashed line) and enthalpy of vaporization for n-heptane (dotted line)[29]. The saturation temperature closely corresponds to the observed onset of nucleate boiling, with the enthalpy of vaporization vanishing as the critical point is approached. The transition boiling regime, which some studies identify, is not classified here due to the difficulty in observing near-wall behavior due to the refractive index gradients near the wall—particularly

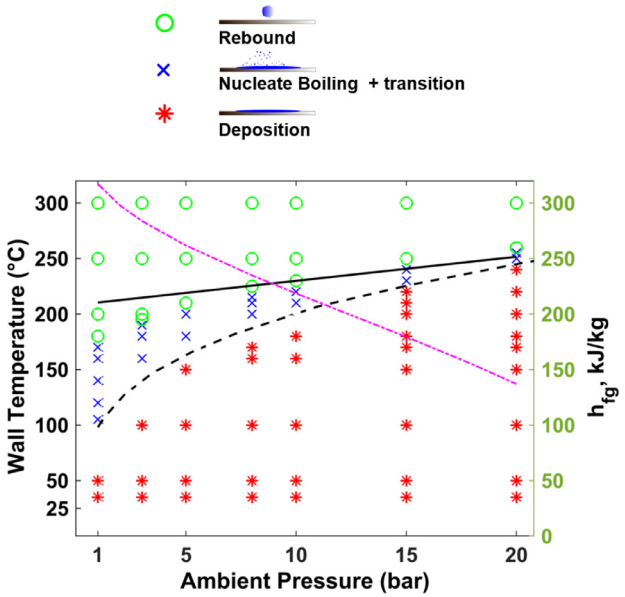

Fig. 5. Regime diagram showing outcomes of n-heptane drop impact for wall temperatures of 35–300 °C and ambient pressures of 1–20 bar. The saturation temperature for n-heptane is indicated by the dashed line. The thermodynamic limit of superheat estimated based on Redlich-Kwong equation of state is shown by solid black line. The variation of the enthalpy of vaporization with ambient pressure is shown by purple dashed line.

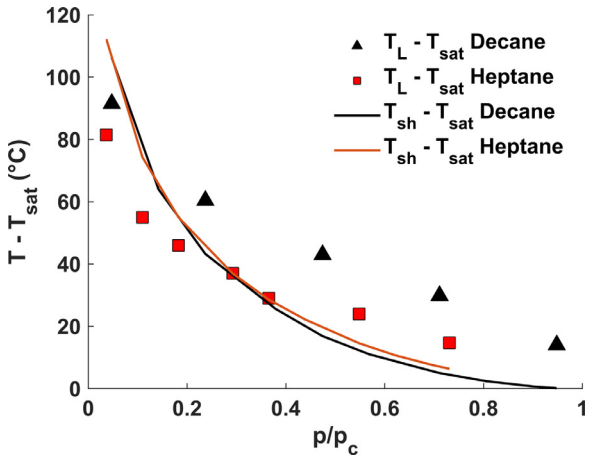

Fig. 6. Symbols represent the difference between the film-boiling inception and saturation temperature ($T_L - T_{sat}$) with varying ambient pressure for n-heptane, n-decane. The two curves indicate the difference between the liquid superheat temperature and saturation temperature ($T_{sh} - T_{sat}$) for the same reduced pressures.

Table 1
Critical temperature and pressure for fluids considered [29].

Substance	Critical Pressure (bar)	Critical Temperature (°C)	Critical Volume (l/mol)
N-heptane	27.4	267	0.428
N-decane	21.1	344.8	0.624

at high pressure conditions. A second thermodynamic limit is considered in the regime diagram shown in Fig. 5: the liquid superheat limit. The superheat limit defines the existence of metastable superheated liquid states, as discussed previously. The superheat limit or liquid spinodal determined from the Redlich-Kwong equation of state is indicated by the solid line in Fig. 5. From the regime map of Fig. 5, the onset of rebound or Leidenfrost temperature is bounded by the liquid spinodal (superheat limit temperature) and liquid binodal (saturation temperature) for n-heptane.

As expected, the region below the saturation temperature results in film evaporation for all ambient pressures. Nucleate boiling is observed for temperatures above the saturation temperature, however at elevated pressures the prevalence of small ejected droplets is decreased. The film boiling regime, which is identified by the inception of rebound of the drop, begins at wall temperature of 180 °C for 1 bar ambient pressure ($T_{sat} = 98.5$ °C). Moving to higher pressure, the difference between the liquid superheat limit and the saturation temperature continues to decrease, and the same trend is evident in the observed onset temperature of drop rebound. At 20 bar, rebound of the drop occurs at a wall temperature of 265 °C ($T_{sat} = 245$ °C). At 15 and 20 bar just before the inception of film boiling, there exists a wall temperature range in which the drop does not fully rebound, but a prominent vertical liquid column forms. This might be classified as a transition drop impact outcome where there exists only partial liquid contact at the wall, but the high-ambient-pressure environment complicates the classification of these transition regions.

As observed in the regime map of Fig. 5, the difference between the saturation temperature (at a given pressure) and the wall temperature at which the onset of film boiling is observed decreases with increasing ambient pressure. This trend for the excess temperature ($T_L - T_{sat}$) is summarized in Fig. 6 for both n-heptane and n-decane, where these n-alkanes represent typical boiling points in multicomponent fuels. Both experimental curves decrease as the critical pressure is approached, but do not reach zero–the wall temperature required for rebound as the critical pressure is approached can remain above the critical temperature due to temperature gradients in the liquid mass and the wall. Also shown are two curves representing the difference between the thermodynamic limit of superheat and saturation temperature ($T_{sh} - T_{sat}$) for both fluids. This difference approaches zero at the critical pressure for both fluids, but falls below the experimental observation by several degrees (°C). As mentioned, this may be attributed to unsteady temperature gradient in the wall and liquid mass during interaction. In addition, two-constant equations of state are not sufficiently accurate for proper estimates of the liquid superheat limit and saturation temperature [23], but give a qualitatively correct trend for the liquid superheat limit. For reference, the critical parameters for both fluids are shown in Table 1 [29].

The degree of superheat for the liquid may also be considered for the dimensionless Jakob number, which represents the fraction of the energy available for the complete phase transition. In the literature, Jakob number has been extensively used to classify liquid breaking mechanism during flash evaporation, explain transition criteria between flashing liquid jet regimes, and establish relationship with the flash evaporation efficiency [24,25]. Fig. 7 shows the experimental Jakob number decreasing to ~ zero as the reduced pressure approaches unity. For n-heptane, Ja and the corresponding Ste at 1 bar are 117.74 and 0.65, respectively, whereas at 20 bar these values are 2.54 and 0.55. In practice, homogeneous nucleation occurs between Ste = 0.5–0.8 [24]. At higher pressure of 20 bar, based on Ja and Ste value (0.55) nucleation is expected to occur supporting the notion of significant phase change. The portion of the drop which is in immediate contact with the hot wall is superheated to result in the formation of a vapor layer even at high ambient pressure. For both n-heptane and n-decane, the Jakob number can thus be used to separate the Leidenfrost (drop rebound) behavior for nucleate boiling. For example, for n-heptane at $p/p_c = 0.4$, $Ja > 30$ implies a film boiling outcome and drop rebound. At any value of $Ja < 10$ at pressure ratio of 0.4, the drop will not rebound. Although the data here is shown only for two pure n-alkanes, this serves as a guideline for multicomponent fuel

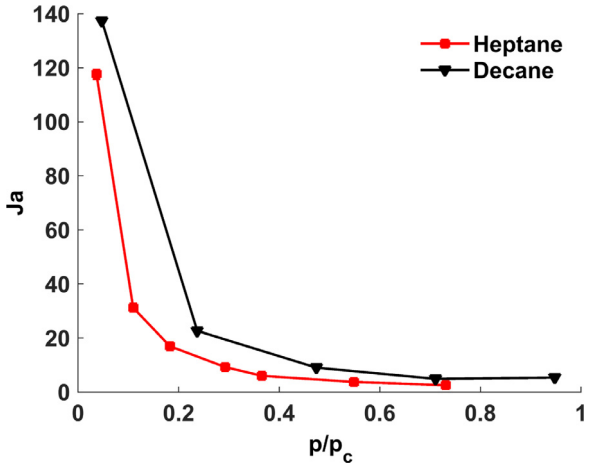

Fig. 7. The onset of Leidenfrost/drop rebound in terms of the dimensionless Jakob number–determined based on the wall temperature and saturation temperature with varying reduced pressure for n-heptane and n-decane. Rebound occurs for points above the curves, while nucleate or film evaporation takes place below the curves.

drops, although additional characterization should be undertaken at relevant ambient pressures for realistic fuel mixtures.

3.2. Drop spreading and rebound characteristics (n-heptane and n-decane)

In addition to the characterization of drop-wall outcomes by behavior, the high-speed image sequences were used to examine the evolution of the drop spreading, rebound, and contact time the the wall. As in the prior section, cases presented are limited to low impact velocity, with a Weber number of ~ 50.

During wall impact, the spreading of the liquid film was examined through the evolution of the speading liquid film diameter, $d(t)$. Both the normalized spread factor ($d(t)/d_0$) and normalized maximum spread (d_{max}/d_0) are shown in Fig. 8. The liquid film spread was defined based on the typical side-view as shown in Fig. 2, with each defined as the liquid film extent as viewed from the side. Panels (a) and (b) shows the variation in spreading of n-heptane for wall temperature cases in the film evaporation regime (100 °C) and film boiling regime (300 °C), respectively, for several ambient pressures. The points indicate the mean value of the normalized spread at a given time instant after impact, with error bars indicating the variance over at least 6 trials. At both low and high wall temperature, the change in the ambient pressure from 1 to 20 bar does not significantly influence the maximum spread, liquid film spread, or the recoil rate for n-heptane. However, at late times, there is a clear trend in both cases: the normalized spread increases with ambient pressure. This is consistent with a decreasing surface tension [30]. In addition, the time of maximum spread is delayed for the 10 and 20 bar ambient pressure cases, as compared to the 1 bar case. This may be attributed to the density ratio of gas to liquid increase of approximately twenty-fold when the pressure is increased to 20 bar—resulting in increased resistance by the dense gas.

To summarize the behavior for both n-heptane and n-decane, the maximum spread factor was determined from the time-resolved spread factor data and is presented in Fig. 8(c). For both n-heptane and n-decane, the maximum spread showed minimal dependence on the ambient pressure. As previously established in literature, the maximum spread of the liquid film is mainly influenced by the liquid surface tension, viscosity, and contact angle [31,32]. The gas viscosity also plays a key role in determining the maximum liquid film spread [33,34]. For a cold wall case, Roisman et al. solved the coupled mass, momentum, and energy balances to predict the dependence of the maximum spread diameter on the Weber and Reynolds numbers in two distinct regimes: capillary and viscous. For the viscous regime, the maximum spread was shown to scale with $Re^{0.2}$ [35]. Another refined model based on the energy balance approach predicts well the maximum spread diameter of a drop as a root of a cubic equation consisting of Weber number, Reynolds number and contact angle [36]. For a heated wall case, Ajaev et al. incorporated coupled effects of evaporation, disjoining pressure, Marangoni stress, surface tension, thermocapillarity and gravity using lubrication approach to conclude that droplet spread depends on the value of superheat [37]. However, these studies were limited to atmospheric ambient pressures. Table 2 presents a detailed comparison between the estimated and experimentally measured values of maximum spread based on two separate cases: hot wall, and cold wall. The values are estimated on the basis of empirical relations proposed in the models. The values normalised by the drop diameter have been employed for the purpose of comparison at 1 bar pressure. Readers can refer to the direct sources for additional details about the model.

To our knowledge, no model exists in the literature to estimate the maximum liquid film spread at higher ambient pressure. For the case of a cold wall, the estimated maximum liquid film spread based on the Tang et al. [38] correlation matches closely with the experimental value of 3.4 ± 0.011. The relation proposed by Tang et al. is a function of Weber and Ohnesorge number and is

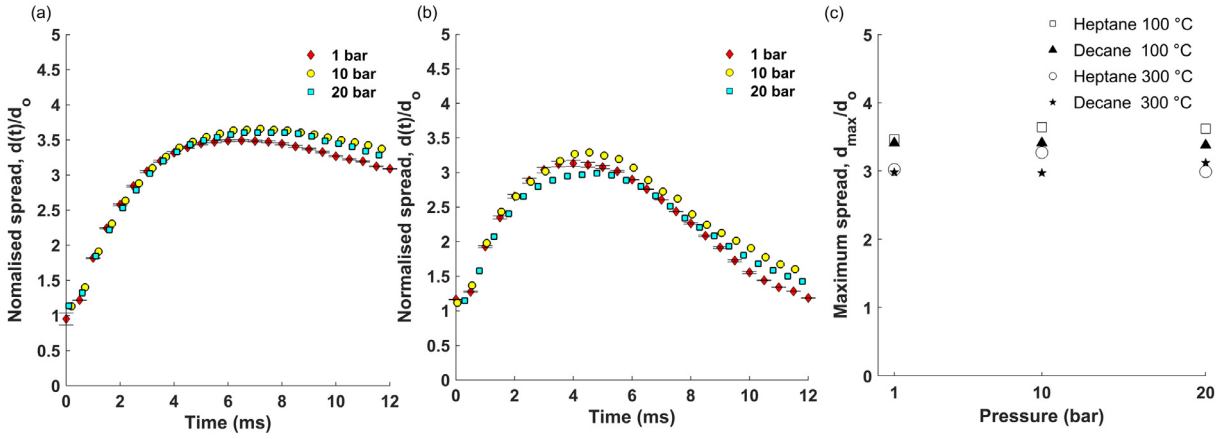

Fig. 8. Time-evolution of liquid film spreading for n-heptane drops at a wall temperature of (a) 100 °C and (b) 300 °C. Error bars indicate the variance in normalized spreading $d(t)/d_0$ over 10 separate impacts. (c) Comparison of maximum spreading of n-heptane and n-decane for a range of wall temperature and ambient pressure conditions.

Table 2
Comparison of experimental maximum liquid film spread with empirical correlations for cold and hot wall conditions for n-heptane.

Cold wall, $T_w = 25°C$				
Reference	Parameters	Conditions	d_{max}/d_0 (Model)	d_{max}/d_0 (Expt. at 1 bar)
Tang et al. [38]	$25 < We < 971$ $2192 < Re < 13495$	Fluid: water, ethanol Surface: SS	3.5	3.4 ± 0.011
Sen et al. [39]	$1 < We < 1000$	Fluid: biofuel Surface: SS	2.99	3.4 ± 0.011
Seo et al. [40]	$12 < We < 1600$ $560 < Re < 15000$	Fluid: gasoline, heptane, ethanol Surface: Al	5.00	3.4 ± 0.011
Roisman et al. [35]	$2 < We < 561$ $670 < Re < 11366$	Fluid: water, glycerin Surface: glass, wax	2.82	3.4 ± 0.011
Chandra et al. [16]	$We = 43,\ Re = 2300$	Fluid: heptane Surface: SS	3.2	3.4 ± 0.011
		Hot wall, $T_w > T_L$		
Reference	Parameters	Conditions	d_{max}/d_0 (Model)	d_{max}/d_0 (Expt. at 1 bar)
Antonini et al. [41]	$1 < We < 100$	Fluid: water, glycol Surface: Al, CO_2(solid)	2.39	3.0 ± 0.0078
Castanet et al. [42]	$4 < We < 160$	Fluid: water, ethanol, water-glycol Surface: Nickel	2.62	3.0 ± 0.0078
Liang et al. [43]	$2 < We < 265$ $111 < Re < 4197$	Fluid: water, ethanol, butanol	2.60	3.0 ± 0.0078
Akao et al. [44]	$2 < We < 600$	Fluid: water, ethanol, acetic acid Surface: Copper	2.90	3.0 ± 0.0078
Chandra et al. [16]	$We = 43,\ Re = 2300$	Fluid: heptane Surface: SS	4.54	3.0 ± 0.0078

applicable for alkanes in the Weber number range of 25 to 971. Several other models for cold wall impact are summarized in the upper rows of Table 2. These predict maximum spreading values from 2.8–5.0, but were developed for a range of fluids and surfaces. On a hot wall (above the Leidenfrost temperature), the existing empirical all models estimate the value close to the experimental value of 3 ± 0.0078. Chandra et al. developed relationship based on a low Weber number and did not consider a wide range of *We* or *Re*. This may have resulted in the over-prediction of the maximum liquid film spread for the cases of interest. For both hot and cold walls, the deviation of the estimated maximum spread value from the measured maximum spread is below 13 %. The existing models satisfactorily predict the maximum liquid film spread for cold and hot wall cases at 1 bar pressure. Since, in our experiments, insignificant influence of ambient pressure was observed, these models can be used to predict maximum liquid film spread in the pressure range of 1–20 bar for n-heptane and n-decane. The comparison also yields another interesting trend which is the lower maximum spread on a hot wall. In our experiments, at 1 bar, the maximum liquid film spread on hot wall is around 11.7 % lower than that on a cold wall. At higher pressures of 10 and 20 bar, maximum liquid film spread is consistently lower than that on a cold wall. The trend of lower maximum liquid film on a hot wall holds even at higher ambient pressures. The result implies that the influence of wall temperature on deciding the liquid spread extent remains dominant in the pressure range of 1–20 bar for n-heptane and n-decane.

Prior experimental studies have shown that wall temperature at which the drop or liquid film starts to levitate varies for an impinging drop, and depends on parameters including the liquid composition, impact momentum, and surface characteristics [10,45]. For these experiments, the drop centroid was identified in the high-speed image sequences, and the rebound duration, velocity, and distance from the wall are shown in Fig. 9 for elevated wall temperature ($T_w = 300$ °C). The upper panel shows the time evolution of the drop distance from the wall, where $t = 0$ ms corresponds to the initial contact as identified by tracking the drop centroid. As evident here, the total duration of contact is determined by the extent of the three curves corresponding to ambient pressures of 1, 10, and 20 bar. Both the time of initial rebound and the total rebound duration are determined from

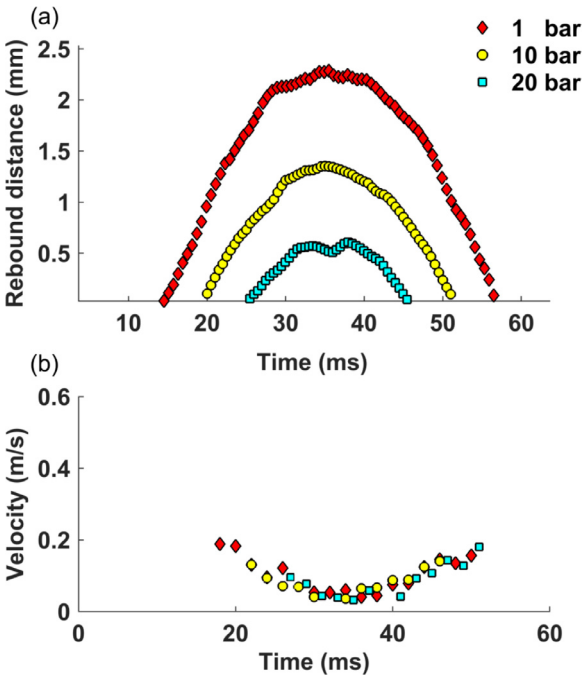

Fig. 9. (a) Rebound distance and (b) rebound velocity for n-heptane drops at ambient pressures of 1, 10, and 20 bar and a wall temperature of 300 °C.

the drop centroid position in the side-view image sequences. For increasing pressure, there is a clear delay in the onset of rebound (60% increase at 20 bar), along with a decreased duration of rebound (60% reduction at 20 bar).

For the same high temperature wall case (300 °C) and pressures, the velocity of the drop centroid is shown in Fig. 9(b). The variation in rebound velocity is similar for all cases of pressure and the values are in the range of 0.05 to 0.2 m/s. The total rebound height and rebound duration are affected by two main factors which are pressure dependent: the evolution of the vapor film at the wall, and increased aerodynamic resistance. For these rebound velocities, drag is negligible, as evident by the velocity evolution

for various ambient pressure conditions. The gas viscosity may have a role to play at low impact velocities, but studies by Xu et al., Stevens et al, suggest important role of the surrounding gas pressure and viscosity in deciding the splashing threshold at moderate and high drop impact velocities [34,46]. Note that as the impact velocity of the drop is increased gradually, the rebound dynamics of the drop changes to splashing producing secondary droplets [13]. The gas pressure surrounding the drop alters the gas viscosity, and therefore considering the gas compressibility in establishing drop dynamics criteria have been suggested in the literature [47].

4. Conclusion

The effect of ambient pressure on the impact sequences of n-heptane and n-decane was presented for an impact Weber number of ~ 50. These results provide a set of validation data for modeling high-temperature, high-pressure drop-wall impingement relevant to spray systems at engine-relevant combustor pressures. The impact sequences of n-heptane drops at wall temperatures of 35–300 °C and ambient pressures of 1–20 bar allowed classification into three distinct outcomes: film evaporation, nucleate boiling, and film boiling where the droplet undergoes complete rebound. The inception of the nucleate boiling regime varies with the liquid saturation temperature, as expected, but we show the Leidenfrost temperature or onset of film boiling is also bounded by the thermodynamic limit of liquid superheat. The degree of superheat for the liquid can be scaled by the enthalpy of vaporization, yielding a criterion for drop rebound as a function of the reduced pressure. We also find that the maximum liquid film spread is not significantly affected by the gas pressure. A quantitative comparison of maximum liquid film spread with existing models shows good agreement with consistently lower maximum spread on hot walls. The rebound dynamics of the drop at different pressure were quantified, and a delay in the inception of the drop rebound is observed when the ambient pressure is raised from 1 bar to 20 bar. The results presented in the study can be used to include ambient pressure effects in developing spray impingement models.

Declaration of Competing Interest

All authors have participated in (a) conception and design, or analysis and interpretation of the data; (b) drafting the article or revising it critically for important intellectual content; and (c) approval of the final version.

This manuscript has not been submitted to, nor is under review at, another journal or other publishing venue.

The authors have no affiliation with any organization with a direct or indirect financial interest in the subject matter discussed in the manuscript

The following authors have affiliations with organizations with direct or indirect financial interest in the subject matter discussed in the manuscript:

Acknowledgments

Funding support was provided by the U.S. Army Combat Capabilities Development Command (CCDC) Army Research Laboratory. Experimental infrastructure was supported in part by the U.S. National Science Foundation (EPS-1101284 and CBET-1332238).

References

[1] M.D. Bassett, J. Hall, M. Warth, Internal combustion engines: performance, fuel economy and emissions, Intern. Combust. Eng. Perform. Fuel Econ. Emissions (2013) 79–91.
[2] M. Saad, Reciprocating internal combustion engines, Thermodyn. Princip. Practice (1997) 390–392, doi:10.1016/B978-0-444-63373-6.00016-2.
[3] A.H. Lefebvre, V.G. McDonell, Atomization and sprays, CRC press, 2017.
[4] M.C. Drake, T.D. Fansler, A.S. Solomon, G. Szekely Jr, Piston fuel films as a source of smoke and hydrocarbon emissions from a wall-controlled spark-ignited direct-injection engine, SAE Trans. (2003) 762–783.
[5] J. Manin, M. Bardi, L.M. Pickett, R. Dahms, J. Oefelein, Microscopic investigation of the atomization and mixing processes of diesel sprays injected into high pressure and temperature environments, Fuel 134 (2014) 531–543.
[6] V. Bertola, An impact regime map for water drops impacting on heated surfaces, Int. J. Heat Mass Transf. 85 (2015) 430–437.
[7] H.J. Staat, T. Tran, B. Geerdink, G. Riboux, C. Sun, J.M. Gordillo, D. Lohse, Phase diagram for droplet impact on superheated surfaces, J. Fluid Mech. 779 (2015).
[8] J. Breitenbach, I.V. Roisman, C. Tropea, Heat transfer in the film boiling regime: single drop impact and spray cooling, Int. J. Heat Mass Transf. 110 (2017) 34–42.
[9] J.D. Bernardin, C.J. Stebbins, I. Mudawar, Mapping of impact and heat transfer regimes of water drops impinging on a polished surface, Int. J. Heat Mass Transf. 40 (2) (1997) 247–267.
[10] A. Chausalkar, S.-C. Kong, J.B. Michael, Multicomponent drop breakup during impact with heated walls, Int. J. Heat Mass Transf. 141 (2019) 685–695.
[11] T. Tran, H.J. Staat, A. Prosperetti, C. Sun, D. Lohse, Drop impact on superheated surfaces, Phys. Rev. Lett. 108 (3) (2012) 36101.
[12] A. Yarin, DROP IMPACT DYNAMICS: Splashing, Spreading, Receding, Bouncing..., Ann. Rev. Fluid Mech. 38 (1) (2006) 159–192, doi:10.1146/annurev.fluid.38.050304.092144.
[13] G.E. Cossali, M. Marengo, M. Santini, Thermally induced secondary drop atomisation by single drop impact onto heated surfaces, Int. J. Heat Fluid Flow 29 (1) (2008) 167–177, doi:10.1016/j.ijheatfluidflow.2007.09.006.
[14] S.-C. Kong, Drop/wall interaction criteria and their applications in diesel spray modeling, Atom. Sprays 17 (6) (2007).
[15] A. Mills, J. Fry, Rate of evaporation of hydrocarbons from a hot surface: Nukiyama and leidenfrost temperatures, Eur. J. Phys. 3 (3) (1982) 152.
[16] S. Chandra, C. Avedisian, On the collision of a droplet with a solid surface, Proc. R. Soc. Lond. A 432 (1884) (1991) 13–41.
[17] R. Temple-Pediani, Fuel drop vaporization under pressure on a hot surface, Proc. Inst. Mech.Eng. 184 (1) (1969) 677–696.
[18] H. HIROYASU, T. KADOTA, T. SENDA, Droplet evaporation on a hot surface in pressurized and heated ambient gas, Bull. JSME 17 (110) (1974) 1081–1087.
[19] G. Emmerson, C. Snoek, The effect of pressure on the leidenfrost point of discrete drops of water and freon on a brass surface, Int. J. Heat Mass Transf. 21 (8) (1978) 1081–1086.
[20] I. Buchmüller, Influence of pressure on Leidenfrost effect, Technische Universität, Darmstadt, 2014 Ph.D. thesis.
[21] J. Bernardin, I. Mudawar, The leidenfrost point: experimental study and assessment of existing models, J. Heat Transf. 121 (4) (1999) 894–903.
[22] M. Blander, J.L. Katz, Bubble nucleation in liquids, AIChE J. 21 (5) (1975) 833–848.
[23] J. Eberhart, The thermodynamic and the kinetic limits of superheat of a liquid, J. Colloid Interface Sci. 56 (2) (1976) 262–269.
[24] T. Bar-Kohany, M. Levy, State of the art review of flash-boiling atomization, Atom. Sprays 26 (12) (2016).
[25] C. Ji, L. Cheng, N. Wang, Z. Liu, Experimental investigation on high-pressure high-temperature spray flash evaporation and the characteristic jakob number, Exp. Therm. Fluid Sci. 102 (2019) 94–100.
[26] I. Roisman, J. Breitenbach, C. Tropea, Thermal atomisation of a liquid drop after impact onto a hot substrate, J. Fluid Mech. 842 (2018) 87–101.
[27] J. Canny, A Computational Approach to Edge Detection, IEEE Trans. Pattern Anal. Mach.Intell. (1986), doi:10.1109/TPAMI.1986.4767851.
[28] B. Gottfried, C. Lee, K. Bell, The leidenfrost phenomenon: film boiling of liquid droplets on a flat plate, Int. J. HeatMass Transf. 9 (11) (1966) 1167–1188.
[29] E.W. Lemmon, I.H. Bell, M.L. Huber, M.O. McLinden, NIST Standard Reference Database 23: Reference Fluid Thermodynamic and Transport Properties-REFPROP, Version 10.0, National Institute of Standards and Technology, 2018. 10.18434/T4JS3C
[30] J. Dechoz, C. Rozé, Surface tension measurement of fuels and alkanes at high pressure under different atmospheres, Appl. Surface Sci. 229 (1–4) (2004) 175–182.
[31] M. Pasandideh-Fard, Y. Qiao, S. Chandra, J. Mostaghimi, Capillary effects during droplet impact on a solid surface, Phys. Fluids 8 (3) (1996) 650–659.
[32] M. Rein, Phenomena of liquid drop impact on solid and liquid surfaces, Fluid Dyn. Res. 12 (2) (1993) 61.
[33] C.S. Stevens, Scaling of the splash threshold for low-viscosity fluids, EPL (Europhys. Lett.) 106 (2) (2014) 24001.
[34] C.S. Stevens, A. Latka, S.R. Nagel, Comparison of splashing in high-and low-viscosity liquids, Phys. Rev. E 89 (6) (2014) 63006.
[35] I.V. Roisman, Inertia dominated drop collisions. ii. an analytical solution of the navier–stokes equations for a spreading viscous film, Phys. Fluids 21 (5) (2009) 52104.
[36] C. Ukiwe, D.Y. Kwok, On the maximum spreading diameter of impacting droplets on well-prepared solid surfaces, Langmuir 21 (2) (2005) 666–673.
[37] V.S. Ajaev, Spreading of thin volatile liquid droplets on uniformly heated surfaces, J. Fluid Mech. 528 (2005) 279–296.
[38] C. Tang, M. Qin, X. Weng, X. Zhang, P. Zhang, J. Li, Z. Huang, Dynamics of droplet impact on solid surface with different roughness, Int. J. Multiphase Flow 96 (2017) 56–69.
[39] S. Sen, V. Vaikuntanathan, D. Sivakumar, Experimental investigation of biofuel drop impact on stainless steel surface, Exp. Therm. Fluid Sci. 54 (2014) 38–46.

[40] J. Seo, J.S. Lee, H.Y. Kim, S.S. Yoon, Empirical model for the maximum spreading diameter of low-viscosity droplets on a dry wall, Exp. Therm. Fluid Sci. 61 (2015) 121–129.
[41] C. Antonini, I. Bernagozzi, S. Jung, D. Poulikakos, M. Marengo, Water drops dancing on ice: How sublimation leads to drop rebound, Phys. Rev. Lett. 111 (1) (2013) 14501.
[42] G. Castanet, O. Caballina, F. Lemoine, Drop spreading at the impact in the leidenfrost boiling, Phys. Fluids 27 (6) (2015), doi:10.1063/1.4922066.
[43] G. Liang, S. Shen, Y. Guo, J. Zhang, Boiling from liquid drops impact on a heated wall, Int. J. HeatMass Transf. 100 (2016) 48–57.
[44] F. Akao, K. Araki, S. Mori, A. Moriyama, Deformation behaviors of a liquid droplet impinging onto hot metal surface, Trans. Iron Steel Inst.Jpn. 20 (11) (1980) 737–743.
[45] J. Breitenbach, J. Kissing, I.V. Roisman, C. Tropea, Characterization of secondary droplets during thermal atomization regime, Exp. Therm. Fluid Sci. 98 (2018) 516–522.
[46] L. Xu, W.W. Zhang, S.R. Nagel, Drop splashing on a dry smooth surface, Phys. Rev. Lett. 94 (18) (2005) 184505.
[47] C. Josserand, S.T. Thoroddsen, Drop impact on a solid surface, Ann. Rev. Fluid Mech. 48 (2016) 365–391.